Journal of Solid State Chemistry **150,** 159–166 (2000)
doi:10.1006/jssc.1999.8572, available online at http://www.idealibrary.com on IDEAL®

New Mixed-Valent Iron (II/III) Phosphates, $Cu_{3-x}Fe_{4+x}(PO_4)_6$

A. A. Belik,* A. P. Malakho,* K. V. Pokholok,* B. I. Lazoryak,*,[1] and S. S. Khasanov†

*Chemical Department, Moscow State University, 119899 Moscow, Russia; and †Institute of Solid State Physics, 142452 Chernogolovka, Russia

Received June 15, 1999; in revised form October 15, 1999; accepted November 5, 1999

The phase formation in the system $Cu_{3-x}Fe_{4+x}(PO_4)_6$ ($0 \le x \le 1$) was investigated at 920°C under air. These phosphates were studied by X-ray powder diffraction and Mossbauer spectroscopy. At $0.3 \le x \le 0.95$ new phosphates, $Cu_{3-x}Fe_{4+x}(PO_4)_6$, are formed which are isotypic with $Fe_7(PO_4)_6$. Mossbauer spectroscopy confirms that the structure stabilizes Fe^{2+} cations up to 19% under air. At $0 \le x < 0.3$ the synthesized specimens contain $Cu_2P_2O_7$, while at $0.95 < x \le 1$ they contain $FePO_4$ as the second phases. The crystal structures of $Cu_{2.4}Fe_{4.6}(PO_4)_6$ and $Cu_{2.05}Fe_{4.95}(PO_4)_6$ specimens were studied by the Rietveld method. They crystallize in the triclinic space group *P*-1 (No. 2), $Z = 1$ with $a = 7.9231(2)$ Å, $b = 9.3099(2)$ Å, $c = 6.2582(2)$ Å, $\alpha = 107.395(2)$, $\beta = 100.980(2)$, $\gamma = 105.675(2)$ for $Cu_{2.4}Fe_{4.6}(PO_4)_6$ and $a = 7.9434(2)$ Å, $b = 9.3089(2)$ Å, $c = 6.2654(2)$ Å, $\alpha = 107.564(2)$, $\beta = 101.040(2)$, $\gamma = 105.643(2)$ for $Cu_{2.05}Fe_{4.95}(PO_4)_6$. The Fe^{3+} cations are localized in $M(2)O_6$ and $M(4)O_6$ sites. The trigonal bipyramidal $M(3)O_5$ sites are fully occupied by Cu^{2+} cations in both structures. With increasing iron content in $Cu_{3-x}Fe_{4+x}(PO_4)_6$, the substitution of Fe^{2+} for Cu^{2+} is realized in $M(1)O_6$ sites. © 2000 Academic Press

Key Words: **phosphates; copper; iron; Mossbauer spectroscopy; crystal structure; Rietveld method.**

1. INTRODUCTION

Iron phosphates have a rich crystal chemistry and numerous practical applications as heterogeneous catalysis (1–3), passivation of metal surfaces (4), and corrosion inhibition (5). They can be used also as sensor materials (6) and as materials for fossil energy conversion (7). These properties result from the fact that iron has two stable oxidation states, +2 and +3.

Gorbunov *et al.* (8) have reported the crystal structure of the mixed-valent iron (II/III) phosphate, $Fe_7(PO_4)_6$. By now a number of isotypic compounds with the general formula $Me_3^{2+}R_4^{3+}(PO_4)_6$ have been described: $Me_3Cr_4(PO_4)_6$ (Me = Cr (9), Zn (9, 10), Mg, Cu (10)), $Me_3Fe_4(PO_4)_6$ (Me = Ni (11), Co (12, 13)), $Mn_2FeFe_4(PO_4)_6$ (13), $Mg_3Ti_4(PO_4)_6$ (14), and $Zn_3V_4(PO_4)_6$ (15). Some hydrogenphosphates, $Co_7H_4(PO_4)_6$ (16), $Mn_7H_4(PO_4)_6$ (17), and $Fe_7H(PO_4)_6$ (18), vanadates, β-$Cu_3Fe_4(VO_4)_6$ (19), $NaCuFe_2(VO_4)_3$ (20), and $LiCuFe_2(VO_4)_3$ (21), and molybdates, $Ag_2Zn_2(MoO_4)_3$ (22) and $Na_2Mg_5(MoO_4)_6$ (23), are crystallized in the same structure type. The composition of iron-containing phosphates, $Me_3Fe_4(PO_4)_6$, differs from stoichiometric. The actual stoichiometry of specimens $Co_3Fe_4(PO_4)_6$ and $Mn_2FeFe_4(PO_4)_6$ defined in the course of the structure refinement was $Co_{2.9}Fe_{4.1}(PO_4)_6$ and $Mn_{2.06}Fe_{4.94}(PO_4)_6$ (13). Mossbauer spectroscopy of cobalt/iron phosphate, $Co_3Fe_4(PO_4)_6$, showed the presence of Fe^{2+} cations (12). The composition of the titled compound, $Ni_3Fe_4(PO_4)_6$, was reported as $Ni_{2.75}Fe_{4.25}(PO_4)_6 + 0.266Ni_{1.81}Fe_{0.19}P_2O_7$ (11).

The $Fe_7(PO_4)_6$ structure type is described in many studies (8–23). The structure contains four independent cation sites, octahedra $M(1)O_6$, $M(2)O_6$, and $M(4)O_6$, and trigonal bipyramid $M(3)O_5$. In the idealized structure the $M(1)$ and $M(3)$ sites are occupied by bivalent cations and the $M(2)$ and $M(4)$ sites are occupied by trivalent cations (10). This distribution was confirmed by the electrostatic site potential calculations (8, 10, 13). Experimental cation distribution has shown that the $M(3)$ site is always occupied by bivalent cations and the $M(4)$ site is always occupied by trivalent cations (10). The $M(1)$ site is preferably occupied by bivalent and the $M(2)$ site by trivalent cations. Disordering of bi- and trivalent cations over the $M(1)$ and $M(2)$ sites was observed for some structures (10, 13, 14). For example, the following cation distribution was found in $Cu_3Cr_4(PO_4)_6$ (10): $0.892Cu^{2+} + 0.108Cr^{3+}$–$M(1)$, $0.054Cu^{2+} + 0.946Cr^{3+}$–$M(2)$, $1Cu^{2+}$–$M(3)$, and $1Cr^{3+}$–$M(4)$.

To our knowledge, only one compound, $Cu_{1.35}Fe_3(PO_4)_3$, with the alluaudite-type structure has been described (24) in the system Cu–Fe–P–O. In this paper, we describe new mixed-valent iron (II/III) phosphates, $Cu_{3-x}Fe_{4+x}(PO_4)_6$, with the $Fe_7(PO_4)_6$ structure type.

2. EXPERIMENTAL

Synthesis

$Cu_{3-x}Fe_{4+x}(PO_4)_6$ ($0 \le x \le 1$) specimens were synthesized from stoichiometric mixtures of CuO, Fe_2O_3, and $NH_4H_2PO_4$ by solid-state method at 900–920°C (90 h,

[1]To whom correspondence should be addressed. E-mail: lazoryak@tech.chem.msu.ru.

0022-4596/00 $35.00

ground every 30 h) under air in alumina crucibles. All starting components were of analytical grade. Specimens with $x = 0$, 0.2, 0.3, 0.4, 0.6, 0.9, and 1.0 were obtained. After annealing, the specimens were quenched at room temperature. The powders with $0 \leq x \leq 0.6$ were dark gray–green and had a different tinge depending on iron content. The specimens with $x = 0.9$ and 1.0 were almost black.

X-Ray Diffraction

X-ray diffraction (XRD) measurements were performed at room temperature on a Siemens D500 powder diffractometer, equipped with an incident-beam SiO_2-monochromator (Cu$K\alpha_1$, radiation at 30 kV and 30 mA, $\lambda = 1.5406$ Å, Ni-filter, Bragg–Brentano geometry) and a position-sensitive detector (BRAUN). XRD data for phase analysis were collected between $2\theta = 10$–60° with a step interval of 0.02°. Effective counting time per step was ca. 5 min. Silicon was used as an external standard. For structure refinements of the $Cu_{2.4}Fe_{4.6}(PO_4)_6$ and $Cu_2Fe_5(PO_4)_6$ specimens, XRD data were collected in the range $2\theta = 10$–120° with a step interval of 0.02°. Effective counting time per step was ca. 30 min. XRD data processing and the structure refinements were carried out by the Rietveld method (25) using the program RIETAN-94 (26).

Mossbauer Spectroscopy

Iron-57 Mossbauer spectra were recorded at room temperature using a constant acceleration Mossbauer spectrometer coupled with a 1024 multichannel analyzer and a ^{57}Co/Cr source kept at RT. All isomer shift values (δ) given hereafter are referred to as α-iron. Experimental data were resolved into symmetric quadrupole doublets with Lorentzian lineshapes using an iterative least-square fit program.

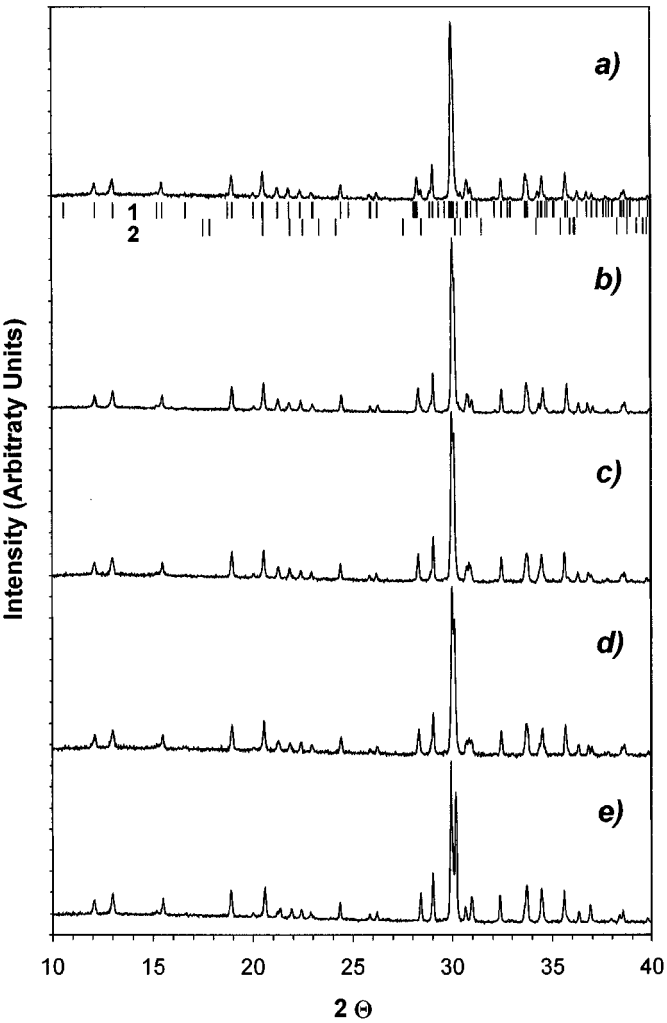

FIG. 1. X-ray diffraction patterns of $Cu_{3-x}Fe_{4+x}(PO_4)_6$ with $x = 0$ (a), 0.2 (b), 0.3 (c), 0.4 (d), 0.9 (e) after the Rietveld processing of XRD data. For the $Cu_3Fe_4(PO_4)_6$ specimen, Bragg reflections of the phase with the $Fe_7(PO_4)_6$ structure type (1) and $Cu_2P_2O_7$ (2) are shown.

3. RESULTS AND DISCUSSION

Phase Analysis

XRD showed that the specimens $Cu_{3-x}Fe_{4+x}(PO_4)_6$ with $x = 0$ and 0.2 contained $Cu_2P_2O_7$ as the second phase. The specimen with $x = 1.0$ contained $FePO_4$ as the second phase. The specimens with $x = 0.3$, 0.4, 0.6, and 0.9 were single phased. The quantity of the second phases was estimated using the RIETAN-94 program (26) by the formula given in (27), which includes the Rietveld scale factors and the crystallographic information about phases. Only unit cell parameters (among all structural parameters) of $Cu_2P_2O_7$ (28), $FePO_4$ (29), and phases which are isotypic with $Fe_7(PO_4)_6$ were refined during Rietveld processing of XRD data. The specimen with the total composition of $Cu_3Fe_4(PO_4)_6$ had ca. 4.4 wt% of $Cu_2P_2O_7$, the specimen with the total composition of $Cu_{2.8}Fe_{4.2}(PO_4)_6$ had ca. 2.0 wt% of $Cu_2P_2O_7$, and the specimen with the total composition of $Cu_2Fe_5(PO_4)_6$ had ca. 2.0 wt% of $FePO_4$. Note that the detection of $FePO_4$ was not possible without the Rietveld processing of XRD data, as the strongest line of $FePO_4$ ($2\theta = 25.84$) coincided with lines of the phase with the $Fe_7(PO_4)_6$ structure type. XRD patterns of $Cu_{3-x}Fe_{4+x}(PO_4)_6$ with $x = 0$, 0.2, 0.3, 0.4, and 0.9 after Rietveld processing are shown in Fig. 1. The refined unit-cell parameters of all phases with the $Fe_7(PO_4)_6$ structure type are given in Table 1.

XRD patterns of $Cu_{3-x}Fe_{4+x}(PO_4)_6$ ($0 \leq x \leq 1$) are slightly distinguished even in the composition region of $0 \leq x \leq 0.3$. It is especially noticeable in the vicinity of the strongest line $2\theta = 29$–31° (Fig. 1). This is probably due to the fact that the system $Cu_{3-x}Fe_{4+x}(PO_4)_6$ is not quasi

TABLE 1
Unit Cell Parameters for Phases With the $Fe_7(PO_4)_6$ Structure Type in $Cu_{3-x}Fe_{4+x}(PO_4)_6$ ($0 \leq x \leq 1$)

x	a, Å	b, Å	c, Å	α	β	γ	V, Å^3
0.0	7.9076(4)	9.3195(6)	6.2558(4)	107.155(9)	100.976(9)	105.752(9)	405.2
0.2	7.8991(4)	9.3102(6)	6.2529(4)	107.219(9)	100.967(9)	105.699(9)	404.2
0.3	7.9275(4)	9.3201(6)	6.2552(4)	107.234(9)	100.993(9)	105.797(9)	405.8
0.4	7.9155(4)	9.3130(6)	6.2549(4)	107.279(9)	100.982(9)	105.730(9)	404.9
0.6	7.9230(4)	9.3092(6)	6.2581(4)	107.390(9)	100.988(9)	105.673(9)	405.2
0.9	7.9395(5)	9.3072(7)	6.2614(5)	107.519(9)	101.031(9)	105.661(9)	405.7
1.0	7.9411(4)	9.3052(6)	6.2639(4)	107.566(9)	101.043(9)	105.647(9)	405.7

binary (iron changes its oxidation state and copper pyrophosphate appears), and the $Fe_7(PO_4)_6$ structure type may contain more (for example, $LiCuFe_2(VO_4)_3$ (21)) or less (for example, $NaZn_{5.5}(MoO_4)_6$ (30)) than 7 cations per unit cell. It seems that the composition of phases which possess the $Fe_7(PO_4)_6$ structure type are distinguished in the region $0 \leq x \leq 0.3$.

The quantity of Fe^{2+} in the mixed phosphates $Cu_{3-x}Fe_{4+x}(PO_4)_6$ depends on the starting stoichiometry. The experimental results showed that the quantity of Fe^{2+} can change in the region $0.3 \leq x \leq 0.95$ and in this region impurity phases are absent. Thus the crystal structure $Cu_{3-x}Fe_{4+x}(PO_4)_6$ stabilizes the Fe^{2+} cations during the synthesis. The only possibility of formation of Fe^{2+} is the lost of oxygen by Fe_2O_3 during synthesis. It is well known that Fe_3O_4 is stable above 1200°C. It seems that the temperature of appearance of Fe^{2+} decreases (up to 900°C) in the $Cu_{3-x}Fe_{4+x}(PO_4)_6$ system during the synthesis.

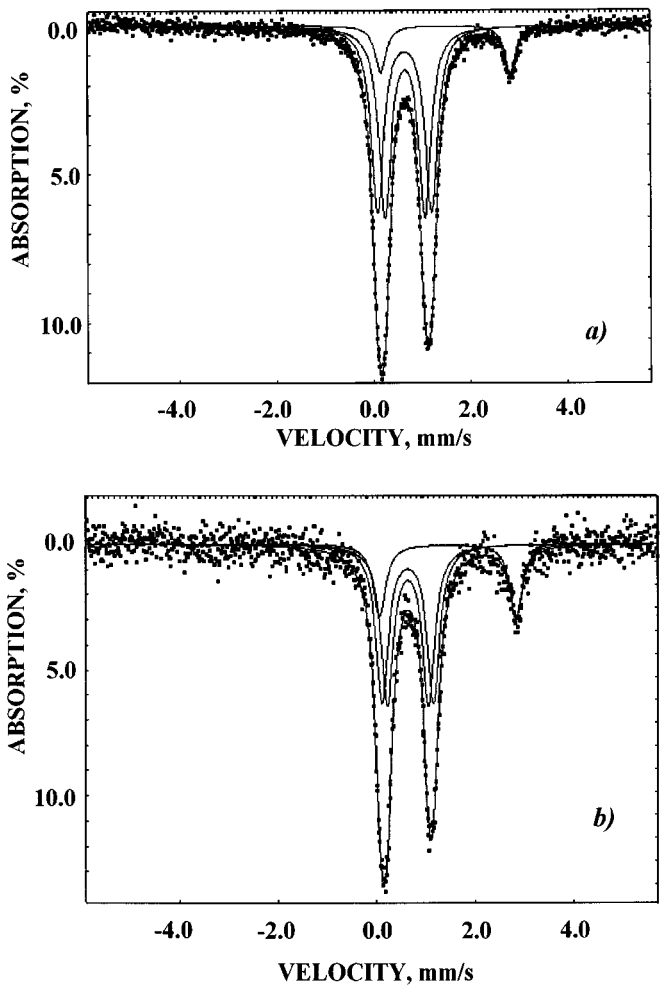

FIG. 2. Mossbauer spectra of (a) $Cu_{2.6}Fe_{4.4}(PO_4)_6$ and (b) $Cu_2Fe_5(PO_4)_6$ specimens at room temperature.

Mossbauer Spectroscopy

Mossbauer spectra of the $Cu_{2.6}Fe_{4.4}(PO_4)_6$ and $Cu_2Fe_5(PO_4)_6$ specimens are shown in Fig. 2 and the parameters corresponding to the fits shown in this figure are given in Table 2. The full line widths at half-maximum (FWHM) of the Fe^{3+} doublets were constrained to be equal during least-square fitting. The fits of the spectra are not unique. The fits are very similar and differ mainly by the parameters of the Fe^{2+} doublets. These parameters vary in

TABLE 2
Parameters of Mossbauer Spectra for $Me_3Fe_4(PO_4)_6$ at Room Temperature

Me	δ^a, mm/s	$\Delta E_Q{}^b$, mm/s	Γ^c, mm/s	S^d, %	Ref.
Co	0.44	0.72	0.48	95	(12)
Ni	0.44(1)	0.61(2)	0.29(1)	52	(11)
	0.44(1)	1.00(2)	0.29(1)	39	
	1.24(3)	2.61(6)	0.47(2)	9	
Fe	0.445	0.53			
	0.445	0.83			(31)
CN = 5	1.12	2.56			
CN = 6	1.31	2.78			
Fe	0.45(1)	0.57(2)	0.29(1)	28 (2)	
	0.45(1)	0.82(2)	0.29(1)	33 (2)	(32)
CN = 5	1.15(1)	2.60(2)	0.24(1)	26 (2)	
CN = 6	1.34(1)	2.85(2)	0.24(1)	13 (2)	
	0.47(1)	0.83(1)	0.30(1)	44.8(15)	
(Cu, Fe)*	0.46(1)	1.12(1)	0.30(1)	45.0(15)	(this work)
	1.31(1)	2.68(1)	0.27(1)	10.2(15)	
	0.47(1)	0.84(1)	0.30(1)	40.6(15)	
(Cu, Fe)**	0.47(1)	1.04(1)	0.30(1)	40.7(15)	(this work)
	1.28(1)	2.78(1)	0.31(1)	18.7(15)	

[a]Chemical shift.
[b]Quadrupole splitting.
[c]Full width at half maximum.
[d]Area.
*The $Cu_{2.6}Fe_{4.4}(PO_4)_6$ specimen (the expected area for Fe^{2+} is 9.1%).
**The $Cu_2Fe_5(PO_4)_6$ specimen (the expected area for Fe^{2+} is 19.2%).

the ranges $\delta = 1.25–1.38$ mm/s and $\Delta = 2.80–2.53$ mm/s for $Cu_{2.6}Fe_{4.4}(PO_4)_6$ and $\delta = 1.28–1.37$ mm/s and $\Delta = 2.78–2.60$ mm/s for $Cu_2Fe_5(PO_4)_6$. It was not possible to choose one model using the "goodness-of-fit" criterion. So we chose the model that gives isomer shifts close to Fe^{2+} (with CN = 6) in $Fe_7(PO_4)_6$ ($\delta = 0.31$ mm/s (31), 0.32 mm/s (11) and 0.34 mm/s (32)) and close to the isomer shift range for Fe^{2+} (with CN = 6) in oxides given by Menil (33) ($1.06 \le \delta \le 1.29$ mm/s). Isomer shifts of doublets assigned to Fe^{3+} for all compounds with the $Fe_7(PO_4)_6$ structure type are very close to each other ($\delta = 0.46(2)$ mm/s, see Table 2). According to Menil (33), the isomer shifts for Fe^{3+} are $0.29 \le \delta \le 0.50$ mm/s for coordination number CN = 6 in oxides and $0.22 \le \delta \le 0.34$ mm/s for CN = 5. The obtained isomer shifts of Fe^{3+} cations in the $Cu_{2.6}Fe_{4.4}(PO_4)_6$ and $Cu_2Fe_5(PO_4)_6$ ($\delta = 0.47(1)$ mm/s) specimens strongly suggest that Fe^{3+} cations are not located in the five-coordinated site $M(3)O_5$.

FWHM of doublets assigned to Fe^{2+} are close to FWHM for the Fe^{3+} doublets and to the instrumental resolution ($\Gamma = 0.25$ mm/s). It is likely to assume that Fe^{2+} cations occupy only one position. The isomer shifts of the Fe^{2+} doublets in $Cu_{2.6}Fe_{4.4}(PO_4)_6$ and $Cu_2Fe_5(PO_4)_6$ are $\delta = 1.31(1)$ and $1.28(1)$ mm/s, respectively. These isomer shifts correspond also to Fe^{2+} with CN = 6 according to Menil (33): $1.06 \le \delta \le 1.20$ mm/s for CN = 5 and $1.06 \le \delta \le 1.29$ mm/s for CN = 6. The information about FWHM and isomer shifts of the Fe^{2+} doublets circumstantially suggests that Fe^{2+} cations are localized in one octahedral site $M(1)O_6$. Note that this conclusion does not depend on the fitting model because all of them give isomer shift of Fe^{2+} $\delta \ge 1.25$ mm/s.

TABLE 3
Important Refined Parameters and Counting Conditions for $Cu_{2.4}Fe_{4.6}(PO_4)_6$ and $Cu_2Fe_5(PO_4)_6$

	$Cu_{2.4}Fe_{4.6}(PO_4)_6$	$Cu_2Fe_5(PO_4)_6$
Space group	*P*-1 (No. 2)	*P*-1 (No. 2)
Z	1	1
2Θ range (°)	10 ÷ 120	10 ÷ 120
Scan step	0.02	0.02
I_{max} (counts)	44758*	25888**
Lattice constants		
a (Å)	7.9231(2)	7.9434(2)
b (Å)	9.3099(2)	9.3089(2)
c (Å)	6.2582(2)	6.2654(2)
α	107.395(2)	107.564(2)
β	100.980(2)	101.040(2)
γ	105.675(2)	105.643(2)
V (Å^3)	405.2	406.1
d_{exp}, d_{calc} (g/cm^3)	3.97(4), 4.01	3.96(4), 3.99
Number of Bragg reflections	1196	1201[a] + 165[b]
Variables		
Structural/others	63/20	63/20
Reliable factors[c]		
R_{WP}; R_P	8.30; 6.24	10.40; 7.40
R_I; R_F	6.73; 3.25	6.58[a]; 3.19[a] 8.87[b]; 3.30[b]
S	3.33	3.25
D-W d	1.40	1.69

[a] $Cu_{2.05}Fe_{4.95}(PO_4)_6$.
[b] $FePO_4$.
[c] Defined as in (26).
*Background was subtracted in 6500 counts.
**Background was subtracted in 4500 counts.

TABLE 4
Atomic Positional and Isotropic Displacement Parameters for $Cu_{2.4}Fe_{4.6}(PO_4)_6$ (I) and $Cu_2Fe_5(PO_4)_6$ (II)

Atom		*x*	*y*	*z*	B_{iso}
M(1)	I	0	0	0	0.5(1)
	II	0	0	0	0.5(1)
M(2)	I	0.4504(6)	0.1185(5)	0.3866(7)	0.1(1)
	II	0.4517(7)	0.1178(6)	0.3840(9)	0.1(1)
M(3)	I	−0.1950(4)	0.2738(4)	0.2658(6)	0.6(1)
	II	−0.1927(5)	0.2750(5)	0.2659(7)	0.7(1)
M(4)	I	−0.2782(5)	−0.4744(5)	0.0474(7)	0.2(1)
	II	−0.2782(6)	−0.4740(6)	0.0488(8)	0.1(1)
P(1)	I	−0.4021(8)	−0.1661(8)	0.096(1)	0.8(2)
	II	−0.403(1)	−0.165(1)	0.099(1)	0.8(2)
P(2)	I	0.2289(8)	0.3732(7)	0.402(1)	0.4(1)
	II	0.227(1)	0.3703(8)	0.398(1)	0.1(2)
P(3)	I	0.1476(9)	−0.2305(8)	0.234(1)	0.7(2)
	II	0.146(1)	−0.2312(9)	0.233(1)	0.6(2)
O(1)	I	0.035(2)	0.242(1)	0.284(2)	0.2(1)
	II	0.034(2)	0.237(2)	0.277(2)	0.2(1)
O(2)	I	−0.461(2)	−0.085(1)	0.318(2)	0.2(1)
	II	−0.460(2)	−0.083(2)	0.321(3)	0.2(1)
O(3)	I	0.278(2)	0.464(1)	0.243(2)	0.2(1)
	II	0.276(2)	0.466(2)	0.249(3)	0.2(1)
O(4)	I	0.357(2)	0.282(1)	0.445(2)	0.2(1)
	II	0.362(2)	0.280(2)	0.443(3)	0.2(1)
O(5)	I	0.264(2)	−0.227(1)	0.466(2)	0.2(1)
	II	0.262(2)	−0.226(2)	0.468(3)	0.2(1)
O(6)	I	−0.443(2)	−0.347(1)	0.068(2)	0.2(1)
	II	−0.445(2)	−0.351(2)	0.068(2)	0.2(1)
O(7)	I	−0.200(2)	−0.080(2)	0.119(2)	0.2(1)
	II	−0.200(2)	−0.080(2)	0.114(3)	0.2(1)
O(8)	I	−0.472(2)	0.160(2)	0.121(2)	0.2(1)
	II	−0.468(2)	0.163(2)	0.121(3)	0.2(1)
O(9)	I	−0.196(2)	0.333(1)	−0.018(2)	0.2(1)
	II	−0.199(2)	0.335(2)	−0.017(3)	0.2(1)
O(10)	I	−0.243(2)	−0.493(2)	0.360(2)	0.2(1)
	II	−0.247(2)	−0.494(2)	0.354(3)	0.2(1)
O(11)	I	0.197(2)	−0.054(1)	0.235(2)	0.2(1)
	II	0.201(2)	−0.055(2)	0.231(2)	0.2(1)
O(12)	I	−0.056(2)	−0.298(1)	0.206(2)	0.2(1)
	II	−0.055(2)	−0.295(2)	0.208(3)	0.2(1)

Note. The *M*(1) site is field by $0.6Fe^{2+} + 0.4Cu^{2+}$ and $1Fe^{2+}$ in $Cu_{2.4}Fe_{4.6}(PO_4)_6$ and $Cu_2Fe_5(PO_4)_6$, respectively. In both structures the *M*(2), *M*(3), and *M*(4) sites are filled by $1Fe^{3+}$, $1Cu^{2+}$, and $1Fe^{3+}$, respectively.

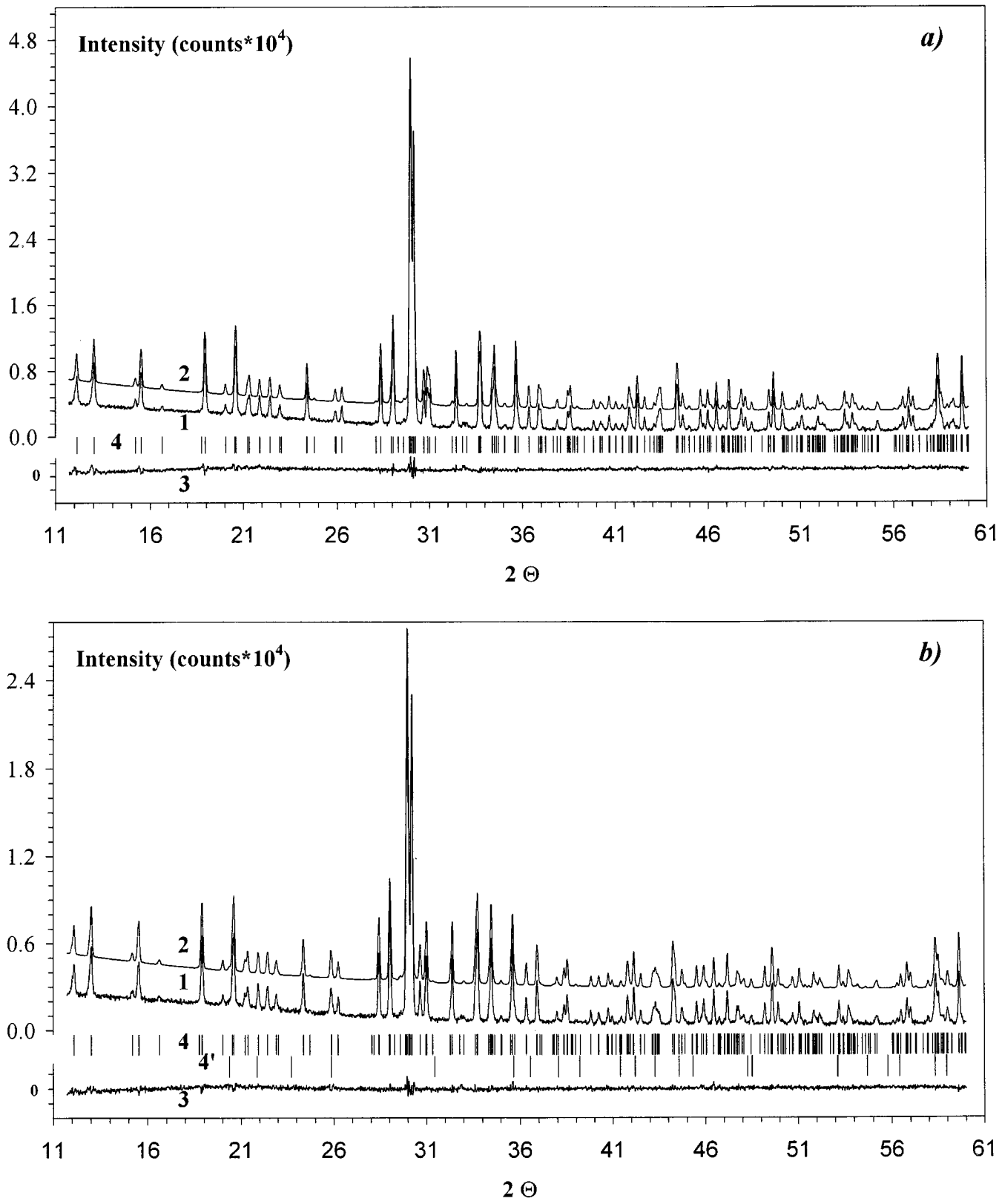

FIG. 3. A portion of the Rietveld refinement profiles for (a) $Cu_{2.4}Fe_{4.6}(PO_4)_6$ and (b) $Cu_2Fe_5(PO_4)_6$; 1, observed; 2, calculated; and 3, difference X-ray powder diffraction patterns; 4 and 4′ Bragg reflections for the phases with the $Fe_7(PO_4)_6$ structure type and $FePO_4$, respectively. The calculated patterns are shifted to 2500 counts from the observed patterns.

As shown in Table 2, the relative areas of the three doublets obtained from a least-square fit agree very well with those calculated from the stoichiometry of the compounds. It is an indication that the recoil-free fractions for the three sites are close. It was expected because the octahedral sites are similar, although no investigation of the temperature dependents of the spectral absorption area was made.

Mossbauer spectroscopy data indicate that iron cations are not localized in the five-coordinated $M(3)$ sites of the structure. Thus, the $M(3)O_5$ sites are fully occupied by Cu^{2+} cations in all compounds and with increasing iron content in $Cu_{3-x}Fe_{4+x}(PO_4)_6$ the substitution of Fe^{2+} for Cu^{2+} is realized in one octahedral site, which is probably $M(1)O_6$.

Structure Refinement

For the structure refinement of the $Cu_{2.4}Fe_{4.6}(PO_4)_6$ and $Cu_2Fe_5(PO_4)_6$ specimens, the atomic coordinates of $Co_3Fe_4(PO_4)_6$ (13) were used as the starting parameters. In the $Cu_2Fe_5(PO_4)_6$ specimen only the scale factor and cell parameters for $FePO_4$ (29) were refined because of its small content (ca. 2 wt%). Counting conditions are given in Table 3. As scattering factors of copper and iron cations are close to each other it was impossible to refine real distribution of these cations over cation sites. Using XRD, it was only possible to examine boundary situations. First, the ideal cation distribution (10) was used; i.e., the bivalent cations were located in the $M(1)O_6$ and $M(3)O_5$ sites and the trivalent cations were located in the $M(2)O_6$ and $M(4)O_6$ sites: $1Fe^{2+}$–$M(1)$, $1Fe^{3+}$–$M(2)$, $1Cu^{2+}$–$M(3)$, and $1Fe^{3+}$–$M(4)$ for $Cu_2Fe_5(PO_4)_6$ and $0.6Fe^{2+} + 0.4Cu^{2+}$–$M(1)$, $1Fe^{3+}$–$M(2)$, $1Cu^{2+}$–$M(3)$, and $1Fe^{3+}$–$M(4)$ for $Cu_{2.4}Fe_{4.6}(PO_4)_6$. According to Mossbauer data the $M(3)O_5$ sites were filled by copper. Using this cation distribution usually observed isotropic thermal displacement parameters (B_{iso}) were obtained for all cations (see Table 4). The following refinement of cation occupancy factors resulted in the values equal to 1 within experimental errors ($n(M(1)) = 1.01(1)$, $n(M(2)) = 1.02(1)$, $n(M(3)) = 1.00(1)$, and $n(M(4)) = 1.02(1)$ for $Cu_2Fe_5(PO_4)_6$ and $n(M(1)) = 1.00(1)$, $n(M(2)) = 1.02(1)$, $n(M(3)) = 1.00(1)$, and $n(M(4)) = 1.01(1)$ for $Cu_{2.4}Fe_{4.6}(PO_4)_6$). When copper cations were placed in the $M(1)$, $M(2)$, or $M(4)$ sites and iron cations were placed in

TABLE 5
Bond Distances (Å) and Angles (°) for Tetrahedra PO_4^{3-} in $Cu_{2.4}Fe_{4.6}(PO_4)_6$ (I) and $Cu_2Fe_5(PO_4)_6$ (II)

Bonds and angles	I	II	Bonds and angles	I	II
P(1)–O(2)	1.59(1)	1.59(2)	P(3)–O(12)	1.52(1)	1.50(2)
–O(8)	1.55(1)	1.56(2)	–O(5)	1.55(1)	1.56(2)
–O(6)	1.56(1)	1.61(2)	–O(9)	1.58(1)	1.61(2)
–O(7)	1.54(1)	1.56(2)	–O(11)	1.58(1)	1.59(2)
⟨P(1)–O⟩	1.56	1.58	⟨P(3)–O⟩	1.56	1.57
O(7)–P(1)–O(2)	112.6(8)	144 (1)	O(5)–P(3)–O(12)	110.8(8)	110.4(9)
–O(8)	109.3(8)	108.7(9)	–O(11)	109.2(8)	109.1(9)
–O(6)	112.3(7)	112.1(9)	–O(9)	110.0(7)	109.8(9)
O(2)–P(1)–O(8)	107.6(7)	108.0(9)	O(12)–P(3)–O(11)	109.0(7)	109.6(9)
–O(6)	106.2(7)	106.6(8)	–O(9)	110.5(8)	112 (1)
O(8)–P(1)–O(6)	108.5(8)	107 (1)	O(11)–P(3)–O(9)	107.2(7)	105.3(8)
⟨O–P(1)–O⟩	109.4	109.4	⟨O–P(3)–O⟩	109.5	109.4
P(2)–O(3)	1.52(1)	1.51(2)	*M*(1)–O(7)*2	1.94(1)	1.93(1)
–O(4)	1.52(1)	1.56(1)	–O(11)*2	2.20(1)	2.21(1)
–O(1)	1.55(1)	1.56(2)	–O(1)*2	2.32(1)	2.26(1)
–O(10)	1.53(1)	1.58(2)	*M*(2)–O(4)	1.84(1)	1.81(1)
⟨P(2)–O⟩	1.53	1.55	–O(8)	1.98(1)	1.99(2)
O(3)–P(2)–O(4)	112.2(8)	112 (1)	–O(11)	2.03(1)	2.02(2)
–O(1)	110.6(8)	111 (1)	–O(2)	1.96(1)	1.96(2)
–O(10)	109.3(8)	107.3(9)	–O(5)	2.10(1)	2.11(2)
O(4)–P(2)–O(1)	104.7(7)	105.4(9)	–O(2′)	2.15(1)	2.12(1)
–O(10)	107.9(8)	106.2(9)	*M*(3)–O(1)	1.91(1)	1.92(2)
O(1)–P(2)–O(10)	112.0(7)	114.1(9)	–O(9)	2.01(1)	2.01(2)
⟨O–P(2)–O⟩	109.5	109.3	–O(5)	1.99(1)	1.99(2)
M(4)–O(12)	1.89(1)	1.91(2)	–O(8)	2.05(3)	2.04(2)
–O(3)	1.85(1)	1.89(2)	–O(10)	2.23(1)	2.23(2)
–O(10)	1.99(1)	1.95(2)			
–O(9)	2.01(1)	2.00(2)			
–O(6)	1.98(1)	1.97(1)			
–O(6′)	2.20(1)	2.18(2)			

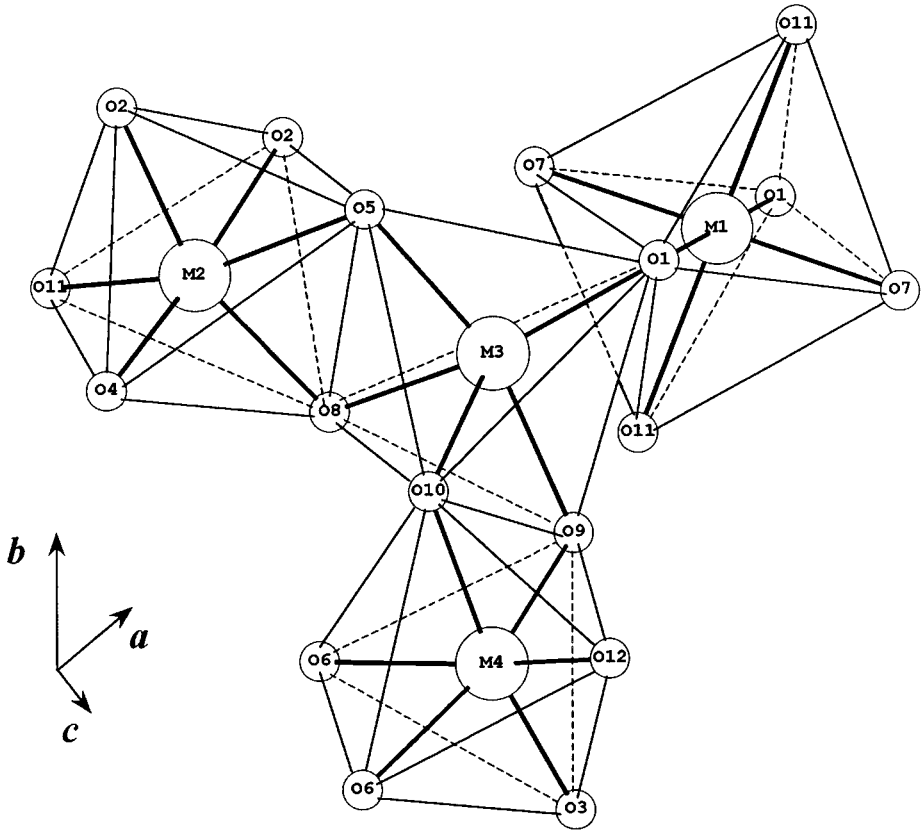

FIG. 4. Polyhedral surrounding of the $M(3)O_5$ site.

the $M(3)$ site in $Cu_2Fe_5(PO_4)_6$, the following occupancies were obtained: $n = 0.91(1)$ for $M(1)$, $M(2)$, or $M(4)$ and $n = 1.09(1)$ for $M(3)$. This result also confirms that Cu^{2+} cations preferably occupy the $M(3)O_5$ sites in $Cu_2Fe_5(PO_4)_6$.

Examination of B_{iso} for $M(1)$–$M(4)$ cation sites in all studied structures of orthophosphates with the $Fe_7(PO_4)_6$ structure type (all of them were obtained using single-crystal data) has shown that B_{iso} for the $M(1)$ and $M(3)$ sites are almost the same, and they are greater than B_{iso} for the $M(2)$ and $M(4)$ sites (which are also almost the same) by a factor 2–3. Despite thermal parameters obtained from powder XRD are less reliable than that obtained from single-crystal data, B_{iso} obtained in this work (Table 4) for the ideal cation distribution is in agreement with this observation. Note that B_{iso} for one and the same site in both structures are equal to each other.

When iron cations were placed in the $M(1)$ sites and $(0.6Fe^{2+} + 0.4Cu^{2+})$ cations were placed in the $M(2)$ or $M(4)$ sites in $Cu_{2.4}Fe_{4.6}(PO_4)_6$ the following occupancies were obtained: $n = 1.04(1)$ for $M(1)$ and $n = 0.95(1)$ for $M(2)$ or $M(4)$ (with fixed B_{iso} as in Table 4). These results confirm that the ideal cation distribution is more probable. Important refinement parameters are given in Table 3. The final observed, calculated, and difference profiles are shown in Fig. 3 and the refined atomic coordinates, thermal parameters, and interatomic distances for $Cu_{2.4}Fe_{4.6}(PO_4)_6$ and $Cu_2Fe_5(PO_4)_6$ are listed in Tables 4 and 5. The main features of the crystal structure are shown in Figs. 4 and 5.

Thus, using both Mossbauer data and XRD structure refinement it was deduced that the trigonal bipyramidal $M(3)O_5$ sites were fully occupied by Cu^{2+} cations in both structures and with increasing of iron content in $Cu_{3-x}Fe_{4+x}(PO_4)_6$ the substitution of Fe^{2+} for Cu^{2+} was realized in the $M(1)O_6$ sites.

Using the results of quantitative phase analysis the composition of the $Cu_2Fe_5(PO_4)_6$ specimen may be presented as $Cu_{2.05}Fe_{4.95}(PO_4)_6 + 0.15FePO_4$. The composition of the phase with the $Fe_7(PO_4)_6$ structure type, $Cu_{2.05}Fe_{4.95}(PO_4)_6$, is very close to the composition of the manganese/iron phosphate, $Mn_{2.04}Fe_{4.96}(PO_4)_6$, which was synthesized by hydrothermal method followed by annealing at 450°C under air for 1 h (13). The $M(1)O_6$ and $M(3)O_5$ sites in $Mn_{2.04}Fe_{4.96}(PO_4)_6$ were found to be occupied by $0.16Fe^{2+} + 0.84Mn^{2+}$ and $0.4Fe^{2+} + 0.6Mn^{2+}$, respectively. This distribution of bivalent cations over the $M(1)O_6$ and $M(3)O_5$ sites differs from the obtained cation distribution in the $Cu_2Fe_5(PO_4)_6$ specimen. The factors

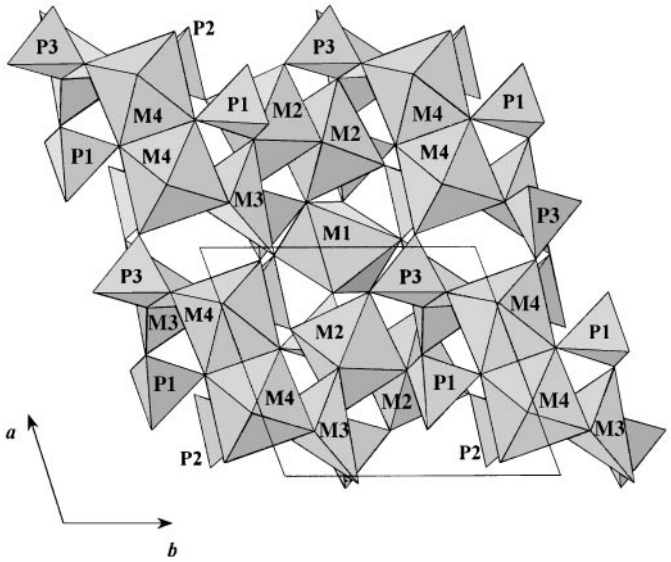

FIG. 5. (001) projection of crystal structure of $Cu_{2.4}Fe_{4.6}(PO_4)_6$.

controlling the distribution of iron and manganese cations in $Mn_{2.04}Fe_{4.96}(PO_4)_6$ remained unclear (13) because Mn^{2+} (d^5) has no site preference on ligand-field grounds, whereas Fe^{2+} (d^6) would be expected to show an octahedral site preference. As for $Cu_{3-x}Fe_{4+x}(PO_4)_6$, iron (II) is localized in the $M(1)O_6$ sites in accordance with ligand-field grounds. Furthermore, the $M(1)O_6$ site is the compressed-octahedral site (see Table 5). Such oxygen coordination is seldom observed for the Jahn–Teller active ion Cu^{2+} (10). This is probably another reason why the substitution of Fe^{2+} for Cu^{2+} is realized in the $M(1)O_6$ sites.

ACKNOWLEDGMENTS

This work was supported by the Russian Fundamental Research Foundation (Grant 97-03-33224a).

REFERENCES

1. J. B. Moffat, *Catal. Rev. Sci. Eng.* **18,** 199 (1978).
2. M. Forissier, D. Foujols, A. Modaressi, and C. Gleitzer, *Bull. Soc. Chim. France* 410 (1985).
3. M. M. Gadgil and S. K. Kulshreshtha, *J. Solid State Chem.* **111,** 357 (1994).
4. S. Attali, B. Vigouroux, M. Lenzi, and J. Persia, *J. Catal.* **63,** 456 (1980).
5. W. Meisel, H. J. Guttmann, and P. Gutlich, *Corros. Sci.* **23,** 1373 (1983).
6. B. I. Lazoryak, *in* "Fundamental Study of New Materials and Processes in the Substance," p. 54. Moscow University Press, Moscow, 1994.
7. M. S. Safonov, B. I. Lazoryak, S. B. Pozharskii, and S. B. Daschkov, *Dokl. Acad. Nauk.* **338,** 633 (1994).
8. Yu. A. Gorbunov, B. A. Maksimov, Yu. K. Kabalov, A. N. Ivaschenko, O. K. Mel'nikov, and N. V. Belov, *Dokl. Acad. Nauk. SSSR.* **254,** 873 (1980).
9. R. Glaum, *Z. Kristallogr.* **205,** 69 (1993).
10. M. Gruss and R. Glaum, *Z. Kristallogr.* **212,** 510 (1997).
11. A. El Kira, R. Gerardin, B. Malaman, and C. Gleitzer, *Eur. J. Solid State Inorg. Chem.* **29,** 1119 (1992).
12. M. R. De Guire, T. R. S. Prasanna, G. Kalonji, and R. C. O'Handley, *J. Am. Ceram. Soc.* **70,** 831 (1987).
13. P. Lightfoot and A. K. Cheetham, *J. Chem. Soc. Dalton Trans.* 1765 (1989).
14. A. Benmoussa, M. M. Borel, A. Grandin, A. Leclaire, and B. Raveau, *J. Solid State Chem.* **84,** 299 (1990).
15. S. Boudin, A. Grandin, A. Leclaire, M. M. Borel, and B. Raveau, *J. Solid State Chem.* **115,** 140 (1995).
16. P. Lightfoot and A. K. Cheetham, *Acta Crystallogr. Sect. C* **44,** 1331 (1988).
17. A. Riou, Y. Cudennec, and Y. Gerault, *Acta Crystallogr. Sect. C* **43,** 821 (1987).
18. I. Vencato, L. D. Moreira, E. Mattievich, and Y. P. Mascarenhas, *J. Brazilian Chem. Soc.* **5,** 43 (1994).
19. M. A. Lafontaine, J. M. Greneche, Y. Laligant, and G. Ferey, *J. Solid State Chem.* **108,** 1 (1994).
20. J. M. Hughes, J. W. Drexler, C. F. Campana, and M. L. Malinconico, *Am. Mineral.* **73,** 181 (1988).
21. A. A. Belik, *Mater. Res. Bull.* **34,** (1999).
22. C. Gicquel-Mayer, M. Mayer, and G. Perez, *Acta Crystallogr. Sect. B* **37,** 1035 (1981).
23. R. F. Klevtsova, V. G. Khim, and P. V. Klevtsov, *Kristallografiya.* **25,** 1148 (1980).
24. T. E. Warner, W. Milius, and J. Maier, *J. Solid State Chem.* **106,** 301 (1993).
25. H. M. Rietveld, *Acta Cryatallogr.* **22,** 151 (1967).
26. F. Izumi, *in* "The Rietveld Method" (R. A. Young, Ed.), Ch. 13. Oxford Univ. Press, New York, 1993.
27. R. J. Hill, *in* "The Rietveld Method" (R. A. Young, Ed.), Ch. 5. Oxford Univ. Press, New York, 1993.
28. H. Effenberger, *Acta Crystallogr. Sect. C* **46,** 391 (1990).
29. G. J. Long, A. K. Cheetham, and P. D. Battle, *Inorg. Chem.* **22,** 3012 (1983).
30. C. Gicquel-Mayer and M. Mayer, *Rev. Chim. Miner.* **20,** 88 (1983).
31. C. Gleitzer, *Eur. J. Solid State Inorg. Chem.* **28,** 77 (1991).
32. A. A. Belik, A. P. Malakho, K. V. Pokholok, and B. I. Lazoryak, *Russ. J. Inorg. Chem.* **44**(9), 1535 (1999).
33. F. Menil, *J. Phys. Chem. Solids* **46,** 763 (1985).